# El Niño phases embedded in Asian and North American drought reconstructions

**Jinbao Li[a,b,*], Shang-Ping Xie[b,c,d], Edward R. Cook[e]**

[a]Department of Geography, University of Hong Kong, Pokfulam, Hong Kong.

[b]International Pacific Research Center, University of Hawaii at Manoa, Honolulu, HI 96815, USA.

[c]Scripps Institution of Oceanography, University of California at San Diego, La Jolla, CA 92093-0230, USA.

[d]Physical Oceanography Laboratory and Ocean–Atmosphere Interaction and Climate Laboratory, Ocean University of China, Qingdao 266100, China.

[e]Lamont-Doherty Earth Observatory, Columbia University, Palisades, NY 10964, USA.

*Corresponding author address:*

Jinbao Li, Department of Geography, University of Hong Kong, Pokfulam, Hong Kong.

Tel.: 852-3917-7101

Fax: 852-2559-8994

Email: jinbao@hku.hk

ABSTRACT

The amplitude of El Niño-Southern Oscillation (ENSO) varies substantially at each phase of its evolution, affecting the timing and patterns of atmospheric teleconnections around the globe. Instrumental records are too short to capture the full behavior of ENSO variability. Here we use the well-validated Monsoon Asia Drought Atlas (MADA) and North America Drought Atlas (NADA) for the past 700 years, and show that tree-ring records from different regions represent tropical sea surface temperature (SST) conditions at various phases of ENSO. Three modes of tree-ring based summer drought variability are found to be correlated with ENSO: summer droughts over the Maritime Continent and Southwest North America (NA), and a dipole mode between Central and South Asia. A lagged correlation analysis is performed to determine the time when precipitation and temperature anomaly imprints on summer droughts as recorded in tree-rings. Drought anomalies in the Maritime Continent and Southwest NA represent ENSO at the developing and peak phases respectively, while those over Central/South Asia are associated with tropical wide SST anomalies (including the Indian Ocean) at the decay phase of ENSO. Thus proxy records from different regions can provide valuable information on long-term behavior of ENSO at different phases.



**Keywords:** ENSO; tree-rings; drought; Monsoon Asia; North America

## 1. Introduction

The El Niño-Southern Oscillation (ENSO) phenomenon dominates tropical ocean-atmosphere variability on interannual timescales, with profound impacts on global weather and climate (McPhaden et al. 2006; Deser et al. 2010). One fundamental property of El Niño, the ENSO warm phase, is that its evolution tends to be phase-locked to the annual cycle, with peak warming around the end of the calendar year (Rasmusson and Carpenter, 1982; Trenberth, 1997). Because of evolving patterns of tropical sea surface temperature (SST) anomalies and atmospheric teleconnections, ENSO effects display strong seasonality in various parts of the globe. Droughts tend to occur in India (Indonesia) in summer (fall) of the El Niño developing year (Shukla and Paolino, 1983; Ropelewski and Halpert, 1987; Haylock and McBride, 2001). Precipitation and temperature anomalies tend to peak over North America during winter at the peak phase of ENSO (Trenberth et al., 1998; Alexander et al., 2002; Johnson and Feldstein, 2010). Warm temperature over India and reduced precipitation over the northwest Pacific east of the Philippines linger through the El Niño decay summer (Xie et al. 2009; Du et al. 2011).

Each El Niño event evolves differently from others, with the amplitude varying substantially throughout the life cycle at the developing, peak, and decay phases (Fig. 1). The large variations in El Niño amplitude, plus the interactions with other climate phenomena such as the Indian Ocean Dipole (IOD), have caused marked changes in ENSO teleconnection patterns around the globe (Krishna Kumar et al. 1999; Annamalai et al., 2005; Xie et al., 2010; Chowdary et al., 2012; Li et al., 2013). Since the 1970s, for example, the ENSO effects weaken on India summer rainfall (Krishna Kumar et al. 1999) but strengthen on Indian Ocean SST and summer rainfall over the northwest Pacific and East Asia (Xie et al. 2010; Chowdary et al. 2012). Therefore, it is important to determine El Niño amplitude variations at each phase of its evolution, a crucial step toward understanding changes in the teleconnection patterns.

Instrumental records indicate that ENSO exhibits strong variability on the classical 2-7-year band in the past 150 years, and that its amplitude and frequency are modulated at decadel to interdecadal timescales (Fang et al., 2008; Deser et al., 2010; Li et al., 2011). In light of such decadel to interdecadal modulation, existing instrumental records are too short to characterize the full behavior of ENSO variability (Guilyardi et al., 2009; Wittenberg, 2009; Yeh et al., 2011; Stevenson et al., 2012). Long integrations of coupled general circulation models (GCMs) have been used to evaluate slow modulations of ENSO (Wittenberg, 2009; Yeh et al., 2011). However, current GCMs have limited ability to reproduce historical ENSO variability, and that they yield a wide range of projections for future ENSO variability (Guilyardi et al., 2009; Yu and Kim, 2010; Ham and Kug, 2012). A better understanding of long-term ENSO variability is necessary for improving climate models and their projection of ENSO behavior linked to global warming.

Proxy records are the primary source to study climate variability beyond the instrumental period. Many proxies, in particular seasonally to annually resolved tree-rings and corals, have been used to reconstruct ENSO variability during the past millennium (e.g., Stahle et al., 1998; Cobb et al., 2003; D’Arrigo et al., 2005; Braganza et al., 2009; Wilson et al., 2010; Emile-Geay et al., 2013; Li et al., 2013). These reconstructions have provided valuable information on long-term ENSO behaviors, such as its frequency change, amplitude modulation, and possible effects of solar and volcanic forcing on ENSO occurrence. Based on various proxy records and statistical methods, however, these reconstructions exhibit large inconsistency in ENSO variability in both low- and high-frequency components (D'Arrigo et al., 2005; McGregor et al., 2010; Wilson et al., 2010).

Part of the ENSO reconstruction uncertainty was introduced by statistical treatment of proxy data (i.e., removal of biological trend in proxies) and/or different method used for each reconstruction (von Storch et al., 2004; Mann et al., 2007; Wilson et al., 2010, Emile-Geay et al., 2013). This type of uncertainty could be minimized by rigorously evaluating and improving the statistical methods (Mann et al., 2007; Smerdon et al., 2010, 2011). Meanwhile, the reconstruction uncertainty was equally likely caused by shifts in ENSO teleconnection patterns, as most of previous studies did not consider seasonal evolution and spatial structure of ENSO and their influence on the spatial/temporal stability of teleconnections (Cole and Cook, 1998; Trenberth and Stepaniak, 2001; Kim et al., 2009). Moreover, proxy records in different regions have distinct phenological cycle, often most sensitive to climate anomalies of a particular season. Without scrutinizing the ENSO signals encoded in proxy records, a simple combination of them for reconstruction will lead to large inconsistencies, a problem that could be worsened by the improper use of statistical techniques. In light of this, we argue that a careful examination of ENSO phases in global proxy records is essential for improving ENSO reconstructions. This assessment is becoming increasingly important, as the need rises to combine and synthesize accurately dated, high-resolution proxy records around the globe.

This study aims to systematically examine the spatiotemporal structures of ENSO effects on summer droughts over Monsoon Asia (MA) and North America (NA), by employing the tree-ring derived Monsoon Asia Drought Atlas (MADA) and North America Drought Atlas (NADA) (Cook et al., 2004, 2008, 2010). This work will pinpoint ENSO phases encoded in tree-rings, and will shed light on the general pattern of tree growth response to ENSO over MA and NA. We hope this work will inspire more exploration of tree-rings and other proxies around the globe to distinguish the encoded ENSO signals. These efforts will eventually lead to more skillful reconstructions to improve our understanding of the complex ENSO system.

The current paper is organized as follows. Section 2 describes instrumental and proxy data as well as the analytical techniques employed in this study. Section 3 describes the two dominant drought patterns over MA and NA for the past seven centuries. In section 4 we demonstrate that the dominant drought patterns over MA and NA are indeed related to different ENSO phases. Section 5 illustrates the seasonal relationships of summer droughts to current and antecedent precipitation/temperature anomalies, and the physical processes for the ENSO-drought connections in each region. Based on the identified phase relationship with ENSO, section 6 discusses the covariability of summer droughts between MA and NA for the past seven centuries. Section 7 is a summary.

## 2. Data and methods

### 2.1. The Monsoon Asia and North America Drought Atlas

We employed the well-validated MADA and NADA to represent climate signals encoded in moisture sensitive tree-rings across the two continents (Cook et al., 2004, 2008, 2010). The MADA and NADA are gridded datasets of tree-ring derived summer (June-August) Palmer Drought Severity Index (PDSI; Palmer, 1965) reconstructions. The PDSI is an index of meteorological drought that incorporates both precipitation and temperature into a two-layer soil moisture reservoir model, such that moisture supply (rainfall or snowfall water equivalent) and demand (water loss through evapotranspiration as a function of temperature) could be accounted for in the model (Palmer, 1965; Heim, 2002). As a means to measure soil moisture content, the PDSI was designed to include a built-in persistence term, which means the PDSI for a given month integrates current and antecedent moisture conditions for a few months to seasons. Moreover, the PDSI is scaled to remove differences between regional climatology, thereby allowing direct comparison of spatiotemporal moisture variations over a large region. By design, positive (negative) values of the PDSI indicate wetter (drier) than normal conditions, generally within a range of –6 to 6. We note a few caveats and limitations on the use of the PDSI, such as its inappropriateness for winter-season and short-term droughts, its slow response to developing and diminishing droughts, and its fixed weighting factors for regions with diverse climatology (Alley 1984; Guttman et al., 1992; Heim, 2002; Wells et al., 2004). Nonetheless, the PDSI remains one of the most widely used drought indices in the United States and for much of the globe (Ntale and Gan, 2003; Dai et al., 2004; Li et al., 2009a; Dai, 2011).

The MADA consists of summer PDSI reconstructions on 534-point grid derived from 327 tree-ring chronologies, available on a 2.5°x2.5° regular grid over MA (Fig. 2). The final MADA product is the ensemble mean of 24-member reconstructions for each grid point using a modified “point-by-point regression (PPR)” method (Cook et al., 1999, 2010). Each PPR model was calibrated over the period 1951-1989, and was verified against instrumental data over 1920-1950 for testing the accuracy of tree-ring estimates. Calibration and verification statistics indicate significant reconstruction skill over most of the domain as far back as 1300. Given that the reconstructions ended in 1989, we appended them with instrumental data from 1990 to 2005, and adjusted the means and variances of the reconstructions accordingly. As a result, the MADA spans 1300-2005 (Fig. 3).

The NADA is a set of tree-ring derived summer PDSI reconstructions over most of NA, based on a 286-point 2.5°x2.5° regular grid (Fig. 2). In its current version (NADAv2a; available online at: http://www.ncdc.noaa.gov/paleo/pdsi.html), the NADA was developed using 1845 annually resolved tree-ring records across Canada, the United States, and northern Mexico (Cook et al., 2008). The PPR method was used in a nested manner in order to utilize the full length of the available tree-ring records to extend the reconstructions as far back as possible (Cook et al., 2004). Each PPR model was developed over the fixed calibration period 1928-1978, and was verified against instrumental PDSI data over 1900-1927. The model test results indicate that the NADA is highly reliable back to 1300, and is still quite useful back to 800. In addition, instrumental PDSI data were appended to the end of the reconstructions to bring them up to 2006. As a result, the NADAv2a covers AD 0-2006, with reconstructions available at over 70% of all grid points during most of the last millennium (Fig. 3). In this study, we focus on the reconstructions over 1300-2005, a period most reliable and consistent with the time span of MADA.

## 2.2. Instrumental climate data

Monthly precipitation and temperature data were obtained from the Climatic Research Unit (CRU) TS 3.1 global climate dataset, available for 1901-2009 on a half-degree grid (Mitchell and Jones, 2005). These climate data were used to investigate how summer droughts over MA and NA are related to current and antecedent precipitation and temperature anomalies.

The primary SST data we used are the National Climatic Data Center (NCDC) extended reconstructed SST dataset version 3b (ERSST.v3b), available on a monthly 2-degree grid (Smith et al., 2008). This dataset starts in 1854, but its variability is heavily damped before 1870 due to sparse data availability. We therefore only used the data after 1870. We repeated our analyses by substituting the ERSST with the Hadley Center and Kaplan SST products (Kaplan et al., 1998; Rayner et al., 2006), and found them very consistent in exhibiting the relationships between global SSTs and drought anomalies over MA and NA. Here we report the results obtained from the ERSST dataset.

### 2.3. Analytical techniques

We adopted an objective approach to investigate the influence of ENSO on summer droughts over MA and NA. That is, we first take advantage of MADA and NADA to define the spatially coherent drought patterns in each continent for the past seven centuries, and then analyze if temporal changes of each drought pattern are related to ENSO variability. This method allows for drought patterns defined in terms of their own long-term spatiotemporal behaviors, avoiding a somewhat arbitrary selection of a region of interest based on its association with ENSO during the instrumental period. This consideration matters in that the ENSO teleconnection patterns might vary over time, and the instrumental data only become available for most of MA untill the 1950s.

Empirical Orthogonal Function (EOF) analysis was used to objectively define the dominant modes of summer drought variability over MA and NA. We performed EOF analysis on MADA and NADA separately, and focused on the first two leading modes in each domain and their temporal variability (i.e., the associated principal components (PCs) of each mode) over 1300-2005.

Because El Niño events are phase-locked to the annual cycle (Fig. 1), summer droughts may result from teleconnections induced by either the preceding or the following El Niño event. In order to pinpoint the influence of ENSO on summer droughts, we investigated their relationships for the full El Niño cycle that spans two calendar years by calculating the seasonally lagged correlations of the MADA/NADA PCs with global SSTs from the precedent to the following winter for their common period 1870-2005. The lagged correlations were presented in a progressive manner, so that the El Niño phases embedded in MADA and NADA could be easily identified.

Summer soil moisture content incorporates climate signals of both current and antecedent seasons (Palmer, 1965; Heim, 2002; St George et al., 2010). In order to unravel physical processes by which ENSO imprints on summer droughts, we calculated the seasonally lagged correlations of the MADA/NADA PCs with the CRU precipitation and temperature data over 1951-2005. These correlations were calculated from the precedent to the following winter, and were presented in a progressive manner. This facilitates identifying the seasonality and the relative role of precipitation versus temperature on summer droughts over MA and NA.

## 3. Dominant drought patterns over MA and NA

### 3.1. Dominant MADA drought patterns

The MADA EOF1 accounts for the largest percentage (15.2%) of variance in the field, and is characterized by a distinct dipole mode, with one center in the mid-latitude Central Asia and the other in India with extensions to the southern Tibetan Plateau and northern

Southeast Asia (Fig. 4A). The EOF loading over Central Asia is much higher than that over South Asia, suggesting that this dipole mode is dominated by moisture variability over Central Asia. The opposite sign of loadings indicates that there exists a seesaw pattern regarding summer moisture change in the two regions, with concomitant moisture increase in Central Asia and a decrease in South Asia, or vice versa. The MADA EOF2 accounts for 9.6% of the total variance, and represents a distinct moisture pattern with strong positive loading over the Maritime Continent (Fig. 4B). The first EOF pattern identified here from standard EOF analysis is nearly identical to the first distinct EOF (DEOF1) mode for the same period (Cook et al., 2010). The second EOF pattern agrees well with the DEOF5 mode in Cook et al. (2010), whereby the explained variance of DEOF5 (6.39%) is as high as that of DEOF2 (6.57%). These agreements suggest that the identified drought patterns for MADA are insensitive to the orthogonality constraint of EOF analysis, and are robust features of summer drought variability over MA, at least for the past seven centuries.

The MADA PC1 represents summer moisture change over Central and South Asia during 1300-2005, with positive scores indicating concomitant pluvials in Central Asian and droughts in South Asia, and vice versa for negative scores (Fig. 5A). The PC scores indicate two pronounced pluvial (drought) conditions over Central (South) Asia around the 1340s-60s and 1420s, both recorded by the Aral Sea sediments in Central Asia (Boomer et al., 2009) and speleothem records in east-central India and west-central China (Zhang et al., 2008; Sinha et al., 2011). These two megadroughts in South Asia indicate severe and sustained monsoon failure during these periods, a vital factor for the demise of the Khmer civilization at Angkor in Cambodia (Buckley et al., 2010). Other megadroughts in South Asia indicated by the MADA PC1, such as those around the 1560s-90s, 1680s-90s, 1760s and 1790s, are widely recorded in ice cores on the southern Tibetan Plateau (Thompson et al., 2000), speleothem records in east-central India and west-central China (Zhang et al., 2008; Sinha et al., 2011), and an independent tree-ring record in southern India (Borgaonkar et al., 2010). The agreement with multiple proxies validates the reliability of MADA PC1 in representing regional moisture change for the past seven centuries.

The MADA PC2 represents summer moisture change over the Maritime Continent, with positive (negative) scores indicating pluvial (drought) conditions, respectively (Fig. 5B). Many of the megadroughts observed in South Asia, such as those around the 1340s-60s, 1420s and 1760s, are also found to occur over Southeast Asia. However, some other megadroughts in South Asia, such as those around the 1560s-90s and 1790s, have no parallels in Southeast Asia. These results suggest that the spatially coherent megadroughts over South and Southeast Asia waxed and waned over time, underlining marked changes in the large-scale circulations of the Asian monsoon system. Future work towards understanding the shifts of these modes will provide deeper insights into the Asian monsoon dynamics. Moreover, a persistent drying trend occurred over Southeast Asia since the 1960s, with its duration and magnitude unprecedented for the past seven centuries (Fig. 5B). This change is likely due to the decrease in both precipitation and SST warming associated with the weakening of the Indo-Pacific Walker circulation (Tokinaga et al., 2012). A similar drying trend is observed in East Asia (Jiang and Wang, 2005; Li et al., 2009b). These persistent drying trends over East and Southeast Asia may suggest a significant weakening of the Asian monsoon system in recent decades, which is thought to be in large part a consequence of global warming (Zhou et al., 2008; Li et al., 2010).

3.2. Dominant NADA drought patterns

The NADA EOF1 accounts for 24.9% of the total variance, and shows a distinct pattern centered over Southwest NA (Fig. 4C). The NADA EOF2 explains 13.7% of the total variance, and is characterized by a dipole mode with opposite loadings over the Pacific Northwest (PNW) and the Texas-Mexico (TexMex) region (Fig. 4D). These two leading EOF patterns for 1300-2005 are nearly identical to the first two EOFs for 1400-2005 using the same dataset (Cook et al., 2011), and are similar to the first and the third mode in a rotated EOF analysis of NADAv1a spanning 1000-2003 (Herweijer et al., 2007). Although there are biological limitations on using total ring-width as a proxy for summer moisture, NADA is capable of representing observed summer droughts over most of western NA (Cook et al., 2004; St George et al., 2010). Therefore, the two identified drought patterns for NADA are likely robust features of summer moisture change over NA, rather than artifacts of tree-ring reconstructions or orthogonality constraint of EOF analysis.

Instrumental records suggest that the 1950s drought is the most severe and prolonged in the Southwest for the 20th century (Fye et al., 2003). The NADA PC1 suggests that this drought is not unprecedented in terms of both severity and duration for the past seven centuries. For example, the droughts in the 1850s-60s and 1660s are comparable to the 1950s drought in severity, and the droughts in the 1360s-1390s and 1560s-1580s had persisted much longer than the 1950s drought (Fig. 5C). In contrast, the early 20th century pluvial recorded by instrumental data is unmatched in both severity and duration for the past seven centuries, despite that several severe and sustained pluvials took place, such as those in the 1300s-1330s and 1820s-30s. These findings from NADA PC1 are consistent with previous studies that use either NADA but with different analytical techniques, or other independent datasets (e.g., Meko et al., 1995; Fye et al., 2003; Woodhouse et al., 2005; Herweijer et al., 2007; Stahle et al., 2007, 2011).

Positive scores of NADA PC2 indicate concomitant pluvials in the PNW and droughts in the TexMex region, and vice versa for negative scores (Fig. 5D). Instrumental data indicate that the 1930s drought is pronounced in the Pacific Northwest for the 20th century (Fye et al., 2003). The NADA PC2 agrees with instrumental data, and provides a longer perspective that the 1930s drought is the worst in the Pacific Northwest for the past seven centuries, although its duration has been exceeded by the 1430s-80s and 1650s-60s drought. Likewise, the early 20th century pluvial is unprecedented in severity for the past seven centuries, though its duration has been surpassed by pluvials around the 1300s-40s and 1590s-1620s. Moreover, a comparison of NADA PC2 with NADA PC1 indicate that many pluvials, such as those around the 1300s-30s, 1590s-1620s, 1820s-30s, 1900s-20s, and many droughts, such as those around the 1430s-70s, 1750s, and 1930s, occurred concomitantly over the Southwest and the Pacific Northwest, whereas opposite moisture conditions took place over the two regions in a few other periods such as the 1410s, 1480s, 1560s-80s, 1950s, and 1990s. These variations in spatially coherent moisture conditions underline marked changes in atmospheric circulations over western NA. As will be discussed in the following section, variations in the spatial coherence of moisture conditions across western NA are mainly due to the shifts in wintertime ENSO teleconnections over the PNW/TexMex region.

## 4. Summer droughts in relation to ENSO phases

Among others, remote SST forcing and regional land-air interactions are two important processes that determine summer moisture condition in a region. SST anomalies in remote oceans can excite or shift large-scale atmospheric circulation patterns, thereby causing precipitation and temperature anomalies that favor the occurrence of droughts or pluvials in different regions (Hoerling and Kumar, 2003; Deser et al., 2010). The land-air interactions involve changes in boundary conditions such as soil moisture and surface albedo, and promote additional precipitation and temperature anomalies that often feedback positively on regional moisture condition (Eltahir, 1998; Pal and Eltahir, 2001; Notaro and Zarrin, 2011). These two processes are intrinsically related, but their relative importance on modulating moisture condition might differ by region. Therefore, in order to pinpoint the influence of ENSO on summer droughts over MA and NA, we will first examine how summer droughts in each region are related to remote SST anomalies (in this section), and then analyze how they are related to regional precipitation and temperature change (in the next section).

The MADA PC1 is most significantly and positively correlated with east-central tropical Pacific SSTs in prior winter (DJF), but their correlations weaken in spring to summer and vanish thereafter (Fig. 6A-F). The progressive weakening of their correlations in antecedent to current seasons indicates that summer drought anomalies over Central/South Asia are most related to the peak phase of El Niño events that develop in the spring to summer of the preceding year and decay in current spring to summer. The positive correlations indicate the occurrence of concomitant pluvials in central Asia and droughts in South Asia when east-central tropical Pacific SSTs are warmer than normal.

In contrast, the MADA PC2 has no significant correlations with east-central tropical Pacific SSTs in prior winter (Fig. 6G). Instead, they are significantly correlated from current spring to the following winter, with the highest correlations in August-October (ASO) (Fig.

6H-L). This seasonality of correlations indicates that summer drought anomalies over the Maritime Continent are most related to the developing phase of El Niño events that peak in the following winter. The negative correlations indicate that droughts occur over the Maritime Continent when east-central tropical Pacific SSTs are warmer than normal.

Similar to MADA PC1, the NADA PC1 is also most significantly and positively correlated with east-central tropical Pacific SSTs in prior winter (DJF), and their correlations weaken in spring to summer and vanish thereafter (Fig. 7A-F). This indicates that summer drought anomalies over Southwest NA are most related to the peak phase of the preceding El Niño event, with wet conditions over the Southwest when east-central tropical Pacific SSTs are warmer than normal.

The NADA PC2 is also most strongly correlated with east-central tropical Pacific SSTs in prior winter (DJF), but the magnitude of correlations is much lower than that for NADA PC1 (Fig. 7G-L). Thus summer drought anomalies over the PNW/TexMex region are weakly related to the peak phase of the preceding El Niño event. The negative correlations indicate the occurrence of concomitant droughts in the PNW and pluvials in the TexMex region when east-central tropical Pacific SSTs are warmer than normal.

Compared to the other three modes, the correlations between NADA PC2 and tropical Pacific SSTs are significant but much weaker, indicating that the ENSO-drought associations might vary over time. We test this possibility by calculating the running correlations between DJF tropical SSTs and each drought mode for successive 31-year intervals during 1870-2005. The results indicate that the ENSO-drought teleconnection is highly persistent over Central/South Asia, the Maritime Continent and Southwest NA during the instrumental period (figures not shown). However, the ENSO-drought teleconnection has varied substantially over the past 136 years over the PNW/TexMex region, with strong association around 1900-30 and weak association around 1960-90 (Supplementary Fig. 1). These results indicate the non-stationary association between ENSO and summer drought anomalies over the PNW/TexMex region.

The association with different ENSO phase for each drought pattern is further assessed by calculating their lead-lag correlations with ENSO indices. Because of the weak and unstable correlations between NADA PC2 and tropical Pacific SSTs, we only calculated 48-month lead-lag correlations between the other three PCs and the Niño3/4 indices for their common period 1870-2005 (Fig. 8). The results indicate that the correlations of each drought pattern with the Niño3/4 indices exhibit similar seasonal evolution, albeit subtle differences exist in the relative magnitude. For MADA PC1, the highest correlations are positive, and are found when ENSO leads by 6-7 months summer droughts over Central/South Asia (Fig. 8A). For MADA PC2, the highest correlations are negative, and are found in the season when ENSO lags by 0-2 months behind summer droughts over the Maritime Continent (Fig. 8B). Similar to MADA PC1, the highest correlations for NADA PC1 are positive, and are found when ENSO leads by 6-7 months summer droughts over Southwest NA (Fig. 8C).

Taken together, the above results indicate that different El Niño phases are embedded in MADA and NADA. Summer droughts over Central/South Asia, Southwest NA, and the PNW/TexMex region are most related to the peak phase of the preceding El Niño event, whereas those over the Maritime Continent are most related to the developing phase of the following El Niño event. Moreover, the ENSO-drought teleconnections are highly persistent over Central/South Asia, the Maritime Continent, and Southwest NA, but they have varied substantially over the PNW/TexMex region, at least for 1870-2005.

## 5. Summer droughts in relation to precipitation/temperature anomalies

Section 4 established that summer droughts over Central/South Asia, the Maritime Continent and Southwest NA are related to different ENSO phases. In this section we analyze how summer droughts in these regions are related to current and antecedent precipitation and temperature anomalies, and discuss physical processes that imprint ENSO effects on local climate/moisture anomalies.

### 5.1. Central/South Asia

The MADA PC1 is positively (negatively) correlated with precipitation over Central (South) Asia from prior winter to current summer, but their correlations vanish in the following autumn to winter (Fig. 9A-F). Consistent correlation patterns are found with the observed summer PDSI (Supplementary Fig. 2), suggesting that tree-rings over Central/South Asia have faithfully reproduced the seasonality and the strength of the observed correlation patterns without significant amplification or dampening effect. Correlations of MADA PC1 with temperature are broadly consistent with that of precipitation, albeit with reversed signs (Fig. 9G-L). Strong correlations of MADA PC1 with precipitation and temperature are both found from April-June (AMJ) to June-August (JJA). In Central Asia, precipitation concentrates in spring to summer, and is light in autumn/winter period (Fig. 9A-F). The season of peak rainfall differs spatially over Central/South Asia, but is generally found in AMJ to JJA (Fig. 9C and 9D). These results indicate that summer moisture over Central/South Asia is tuned mainly to precipitation and temperature anomalies in the major wet season.

The above results indicate that both precipitation and temperature are important for summer drought anomalies over Central/South Asia. This raises a question of whether they contribute independently, or one is simply a covariate of another. To examine whether precipitation and temperature are independent casual factors for summer droughts, we calculated their point-by-point correlations in space, with a focus on the season when they are strongly related to summer droughts. The results indicate that precipitation and temperature in AMJ are closely related to each other over Central/South Asia (Supplementary Fig. 4A), such that their anomalies are largely due to the same forcing. From late spring through summer over transition zones between wet and arid regions, soil moisture controls surface evaporation. The strong soil moisture feedback during this time makes surface air temperature sensitive to antecedent and current precipitation (Guo et al. 2012), and surface cooling occurs in response to excessive antecedent and current precipitation, consistent with our results in Fig. 9.

The MADA PC1 is highly correlated with Niño3/4 SST 6-7 months in advance (equivalent to the preceding NDJ), but their correlations are weak at 0-2 months lead (Fig. 8A). This is because ENSO peaks in NDJ and decays substantially by AMJ/JJA (Fig. 1). Thus the high correlation between MADA PC1 and precipitation/temperature in AMJ/JJA indicates that the ENSO influence on summer droughts over Central/South Asia is likely indirect, mediated by SST anomalies outside the Niño3/4 region. The delayed Indian Ocean warming in response to El Niño is a good candidate. Recent studies indicate that the Indian Ocean SST warming persists well into summer (Du et al., 2009), and is influential on climate of the northwest Pacific and East Asia (Xie et al., 2009; Du et al., 2011; Huang et al., 2010). Our results suggest that this Indian Ocean capacitor effect extends to Central Asia (Li et al., 2010; Fang et al., 2011). Analysis to be presented elsewhere implicates orographic effects by the Tibetan Plateau in response to circulation anomalies associated with the tropical tropospheric warming (Y. Kosaka, personal communications). Over South Asia, the correlations of MADA PC1 are much higher with air temperature (~0.6, Fig. 9I) than with precipitation (~-0.3, Fig. 9C), indicating the importance of the persistent SST warming over the North Indian Ocean and South China Sea for summer dry conditions. Together, these results indicate that although correlated with the peak phase ENSO in the preceding winter, the MADA PC1 actually records tropical-wide SST conditions during the ENSO-decay spring/summer, not just over the equatorial Pacific but including the Indian Ocean and South China Sea.

### 5.2. Maritime Continent

Correlations of MADA PC2 with precipitation in antecedent seasons are generally weak over the Maritime Continent (Fig. 10A-C). Instead, they are strongly and positively correlated in current summer and thereafter (Fig. 10D-F). The seasonality of MADA PC2 correlations with temperature is broadly consistent with that of precipitation (Fig. 10G-L), and is also consistent with local SST anomalies over the North Indian Ocean and South China Sea (Fig. 6G-L). The highest correlations of MADA PC2 with precipitation and temperature are both found in current summer (JJA) (Fig. 10D and 10J). In JJA, the correlations between precipitation and temperature are generally insignificant (Supplementary Fig. 4B), suggesting that they may contribute independently to regional summer drought anomalies.

For the Maritime Continent, the major rainy season differs spatially, but peak rainfall generally occurs in DJF when the Southern Hemisphere summer monsoon prevails (Haylock and McBride, 2001; Hendon, 2003; Chang et al., 2005), with JJA the dry season for most of the region (Fig. 10A-F). The MADA PC2 is highly correlated with Niño3/4 SST in summer to autumn (Fig. 8B). Therefore, the peak correlation between MADA PC2 and precipitation in JJA indicates the direct influence of the developing phase of ENSO on summer droughts over the Maritime Continent.

The Maritime Continent is located in the ascending limb of Walker circulation. In peak wet season (DJF), the prevailing Southern Hemisphere summer monsoon is perturbed by local complex topography, such that rainfall anomalies are not well organized in space over the region (Haylock and McBride, 2001; Hendon, 2003; Chang et al., 2005). In contrast, rainfall variability in summer to autumn occurs in response to atmospheric circulation anomalies associated with ENSO, with high spatial coherence that allows soil moisture to develop analogous patterns over a large region. The highest correlations between MADA PC2 and ENSO are found in ASO (Fig. 6K), consistent with the fact that the ENSO influence on rainfall over the Maritime Continent is most significant in boreal autumn (Haylock and McBride, 2001; Hendon, 2003; Chang et al., 2005).

### 5.3. Southwest North America

The NADA PC1 is positively correlated with precipitation over Southwest NA. The correlations peak in prior winter (DJF; ~0.5), decay toward current summer, and vanish in the following autumn to winter (Fig. 11A-F). Consistent correlation patterns are found with the observed summer PDSI (Supplementary Fig. 3), suggesting that tree-rings have faithfully reproduced the seasonality of the observed correlation patterns. By contrast, the correlations of NADA PC1 with temperature are negative, and peak in AMJ to JJA (~-0.5) instead of DJF (Fig. 11G-L).

The above results indicate that both precipitation and temperature are important for summer droughts over Southwest NA, albeit in different seasons. Because winter/spring precipitation may be stored as snowpack and soil moisture that carry over into subsequent seasons (Pal and Eltahir, 2001; Wu and Kinter III, 2009; Notaro and Zarrin, 2011), surface air temperature (SAT) response to precipitation may be lagged by several months. Therefore, we examined the correlations between December-May precipitation and JJA SAT over the Southwest. The results indicate that their correlations are generally insignificant (Supplementary Fig. 4C), suggesting that they may contribute independently to summer drought anomalies over the region.

Both observed summer PDSI and tree-ring reconstructions cannot resolve summer monsoon rainfall over Southwest NA, and instead they are mainly tuned to winter/spring precipitation (Supplementary Fig. 3). Probable reasons include the coarse resolution of the PDSI grid, high evaporation loss in summer, and the nature of higher inter-annual rainfall variability in winter than in summer (St George et al., 2010). Regardless, NADA is capable of tracking winter precipitation that is most strongly related to El Niño variability. These results are consistent with the fact that ENSO teleconnections via the Pacific-North America (PNA) pattern are strongest in boreal winter (Trenberth et al., 1998; Alexander et al., 2002; Johnson and Feldstein, 2010).

Because of weak correlations between December-May precipitation and JJA SAT, the possibility of direct teleconnections from the tropical Pacific to the Southwest during the ENSO decay spring/summer cannot be completely ruled out and needs further investigation.

Precipitation correlations with NADA PC1 remain high (>0.3) in the southern Rockies in AMJ (Fig. 11C), and are marginally significant (~0.3) on the Great Plains in JJA (Fig. 11D). Further studies are necessary to determine the relative importance of direct tropical teleconnection versus soil moisture feedback for precipitation anomalies in spring/summer of the ENSO decay year.

**6. Covariability between summer droughts over MA and NA**

Recent studies indicate that there exists concomitant summer drought variability between MA and NA (e.g., Lau and Weng, 2002; Hoerling and Kumar, 2003; Seager et al., 2005; Zhao et al., 2011). However, these studies are based on instrumental or reanalysis data, too short to characterize their long-term relationship. Here we employ MADA and NADA to investigate covariability of the dominant drought patterns over MA and NA for the past seven centuries, and discuss their relationship in the context of ENSO forcing.

The concurrent correlations of MADA PC2 with the other three PCs over 1300-2005 are nearly zero, largely because MADA PC2 is related to the developing phase of the following El Niño event, whereas the other three PCs are related to the peak phase of the preceding El Niño event (section 4). In light of this, we shifted MADA PC2 one year forward so that it correlates with the same ENSO events as other PCs. Accordingly, common period for their cross-correlations is adjusted to 1301-2005.

NADA PC1 is positively correlated with MADA PC1 and negatively with MADA PC2 (Table 1), suggesting that there are concomitant pluvials over Central Asia/Southwest NA and droughts over the Maritime Continent/South Asia when east-central tropical Pacific SSTs are warmer than normal. However, as revealed by their 31-year running correlations, the covariability of summer droughts between MA and Southwest NA is not always significant over the past seven centuries, with marked modulation at interdecadal timescales (Fig. 12A). A comparison with the reconstructed ENSO variance series (Fig. 12B; Li et al., 2013) indicates that their covariability is generally strong (weak) when the ENSO variance is high (low), with each high/low-coherence epoch lasting for several decades. Therefore, the covariability of summer droughts between MA and Southwest NA is likely modulated by interdecadal changes in ENSO variance and associated teleconnections.

In contrast, the correlations of NADA PC2 with MADA PC1/PC2 are generally weak (Table 1), so are their 31-year running correlations (results not shown). These results suggest that there are no strong covariability between summer droughts in MA and the PNW/TexMex region over the past seven centuries, despite a few coincident droughts and pluvials in individual years or short intervals (Hoerling and Kumar, 2003; Cook et al., 2010; Zhao et al., 2011). These results are consistent with our early findings that the ENSO teleconnections are stationary over MA but non-stationary over the PNW/TexMex region (Li et al., 2013). Therefore, the concurrent drought anomalies in MA and the PNW/TexMex region are non-stationary and may only occur when the ENSO teleconnections are strong in both regions.

## 7. Summary

We have performed a pioneering study to examine ENSO phases embedded in summer droughts over MA and NA by employing the tree-ring based MADA and NADA. Our results indicate that summer droughts over MA and NA display distinct modes, each responding to a distinct phase of ENSO. For Central/South Asia, summer droughts are most correlated with tropical Pacific SSTs at the peak phase of ENSO in prior winter (DJF). Regional precipitation and temperature anomalies occur one or two seasons later in late spring to early summer. The time delay indicates that the ENSO effects are indirect and are probably due to the Indian Ocean capacitor effect. For the Maritime Continent, the developing phase ENSO affects summer droughts most, through concurrent precipitation and temperature anomalies. For Southwest NA, the peak phase ENSO in prior winter has the most significant influence on summer droughts through winter precipitation. For the PNW/TexMex region, the peak phase ENSO in prior winter has a weak influence on summer droughts but its influence on winter precipitation is non-stationary. The ENSO effects persist through spring/summer over most of western NA, owing to the varied contributions of direct tropical teleconnection and regional snowpack-soil moisture feedback in ENSO decay seasons. Further studies are necessary to determine their relative importance over the region.

The above results illustrate the importance of determining the time when precipitation and temperature imprint on summer droughts. For example, although summer droughts over Central/South Asia and Southwest NA are both most related to the peak phase of ENSO in the preceding winter, the timing of strongest precipitation anomalies leads us to conclude that those in Southwest NA record ENSO teleconnections at the peak phase of ENSO, while those in Central/South Asia represent tropical-wide SST conditions at the decay phase of ENSO.

Our findings reported here provide a framework for future efforts aiming at reconstructing ENSO variability more accurately. For example, tree-rings in Southwest NA might be more useful for reconstructing the peak phase ENSO variability, whereas those in the Maritime Continent might be more appropriate for reconstructing the developing phase ENSO variability. If tree-rings in MA and NA are to be jointly used in studying ENSO it is important to shift by one year those from the Maritime Continent as they respond to the ENSO events that develop in the year of tree-ring formation, whereas those in Central/South Asia and Southwest NA respond to the ENSO events that decay in the year of tree-ring formation. In light of this, more assessment of ENSO phases encoded in tree-rings and other proxies around the world is necessary and shall lead to more skillful multi-proxy reconstructions that will improve our understanding of the complex ENSO system.

**Acknowledgements**

We acknowledge the researchers who have contributed their tree-ring data for the development of MADA and NADA. This research was funded by the National Science Foundation, the National Basic Research Program of China (2012CB955600), the National Oceanic and Atmospheric Administration, the Japan Agency for Marine-Earth Science and Technology, and the Hui Oi-Chow Trust Fund. This is an International Pacific Research Center/School of Ocean and Earth Science and Technology Contribution (###/####) and a Lamont–Doherty Earth Observatory Contribution (####).

**References**

Alexander, M.A., Blade, I., Newman, M., Lanzante, J.R., Lau, N.-C., Scott, J.D., 2002. The atmospheric bridge: The influence of ENSO teleconnections on air–sea interaction over the global oceans. Journal of Climate 15, 2205–2231.

Alley, W.M., 1984. Palmer Drought Severity Index: Limitations and assumptions. Journal of Climate and Applied Meteorology 23, 1100–1109.

Annamalai, H., Xie, S.-P., McCreary, J.P., Murtugudde, H.R., 2005. Impact of Indian Ocean sea surface temperature on developing El Nino. Journal of Climate 18, 302-319.

Boomer, I., Wünnemann, B., Mackay, A.W., Austin, P., Sorrel, P., Reinhardt, C., Keyser, D., Guichard, F., Fontugne, M., 2009. Advances in understanding the late Holocene history of the Aral Sea region. Quaternary International 194, 79–90.

Borgaonkar, H.P., Sikder, A.B., Ram, S., Pant, G.B., 2010. El Niño and related monsoon drought signals in 523-year-long ring width records of teak Tectona grandis L.F. trees from south India. Palaeogeography Palaeoclimatology Palaeoecology 285, 74-84.

Braganza, K., Gergis, J.L., Power, S.B., Risbey, J.S., Fowler, A.M., 2009. A multiproxy index of the El Nino-Southern Oscillation, A.D. 1525-1982. Journal of Geophysical Research 114, D05106, doi:10.1029/2008JD010896.

Buckley, B.N., et al., 2010. Climate as a contributing factor in the demise of Angkor, Cambodia. Proceedings of the National Academy of Sciences. 107, 6748–6752.

Chang, C.P., Wang, Z., McBride, J., Liu, C.H., 2005. Annual cycle of Southeast Asia - Maritime continent rainfall and the asymmetric monsoon transition. Journal of Climate 18, 287–301.

Chowdary, J.S., Xie, S.-P., Tokinaga, H., Okumura, Y.M., Kubota, H., Johnson, N.C., Zheng, X.-T., 2012. Inter-decadal variations in ENSO teleconnection to the Indo-western Pacific for 1870-2007. Journal of Climate 25, 1722–1744.

Cobb, K., Charles, C., Cheng, H., Edwards, R., 2003. El Niño/Southern Oscillation and tropical Pacific climate during the last millennium. Nature 424, 271–276.

Cook, B.I., Cook, E.R., Anchukaitis, K.J., Seager, R., Miller, R.L., 2011. Forced and unforced variability of twentieth century North American droughts and pluvials. Climate Dynamics 37, 1097–1110.

Cook, E.R., Meko, D.M., Stahle, D.W., Cleaveland, M.K., 1999. Drought reconstructions for the continental United States. Journal of Climate 12, 1145–1162.

Cook, E.R., Woodhouse, C.A., Eakin, C.M., Meko, D.M., Stahle, D.W., 2004. Long-term aridity changes in the western United States. Science 306, 1015-1018.

Cook, E.R. et al., 2008. North American Summer PDSI Reconstructions, Version 2a. IGBP PAGES/World Data Center for Paleoclimatology Data Contribution Series # 2008-046.

Cook, E.R., Anchukaitis, K.J., Buckley, B.M., D'Arrigo, R.D., Jacoby, G.C., Wright, W.E., 2010. Asian monsoon failure and megadrought during the last millennium. Science 328, 486–489.

Cole, J.E., Cook, E.R., 1998. The changing relationship between ENSO variability and moisture balance in the continental United States. Geophysical Research Letters 25, 4529 - 4532.

Dai, A., Trenberth, K.E., Qian, T., 2004. A global dataset of Palmer Drought Severity Index for 1870–2002: relationship with soil moisture and effects of surface warming. Journal of Hydrometeorology 5, 1117–1130.

Dai, A., 2011. Characteristics and trends in various forms of the Palmer Drought Severity Index PDSI during 1900-2008. Journal of Geophysical Research 116, D12115, doi:10.1029/2010JD015541.

D'Arrigo, R., Cook, E.R., Wilson, R.J., Allan, R., Mann, M.E., 2005. On the variability of ENSO over the past six centuries. Geophysical Research Letters 32 L03711, doi:10.1029/2004GL022055.

Deser, C., Alexander, M.A., Xie, S.-P., Phillips, A.S., 2010. Sea Surface Temperature Variability: Patterns and Mechanisms. Annual Review of Marine Sciences 2, 115-143.

Du, Y., Xie, S.-P., Huang, G., Hu, K., 2009. Role of air-sea interaction in the long persistence of El Nino-induced North Indian Ocean warming. Journal of Climate 22, 2023–2038.

Du, Y., Yang, L., Xie, S.-P., 2011. Tropical Indian Ocean influence on Northwest Pacific tropical cyclones in summer following strong El Nino. Journal of Climate 24, 315–322.

Eltahir, E.A.B., 1998. A soil moisture-rainfall feedback mechanism. 1: Theory and observations. Water Resource Research 34, 765–776.

Emile-Geay, J., Cobb, K., Mann, M. Wittenberg, A.T., 2013. Estimating central equatorial Pacific SST variability over the past millennium. Part 2: Reconstructions and uncertainties. Journal of Climate 26, 2329–2352.

Fang, K., Gou, X., Chen, F., Li, J., Zhou, F., Li, Y., 2011. Covariability between tree-ring based precipitation reconstructions in Northwest China and sea surface temperature of Indian and Pacific oceans. Climate Research 49, 17–27.

Fang, Y., Chiang, J.C.H., Chang, P., 2008. Variation of mean sea surface temperature and modulation of El Niño–Southern Oscillation variance during the past 150 years. Geophysical Research Letters 35, L14709, doi:10.1029/2008GL033761.

Fye, F., Stahle, D.W., Cook, E.R., 2003. Paleoclimatic analogs to 20th century moisture regimes across the USA. Bulletin of the American Meteorological Society 84, 901–909.

Guilyardi, E., Wittenberg, A., Fedorov, A., Collins, M., Wang, C., Capotondi, A., van Oldenborgh, G.J., Stockdale, T., 2009. Understanding El Niño in ocean-atmosphere general circulation models: progress and challenges. Bulletin of the American Meteorological Society 90, 325–340.

Guo, Z., Dirmeyer, P.A., DelSole, T., Koster, R.D., 2012. Rebound in atmospheric predictability and the role of the land surface. Journal of Climate 25, 4744–4749.

Guttman, N.B., Wallis, J.R., Hosking, J.R.M., 1992. Spatial comparability of the Palmer drought severity index. Water Resource Bulletin 28, 1111–1119.

Ham, Y.-G., Kug, J.-S., 2012. How well do current climate models simulate two types of El Nino? Climate Dynamics 39, 383–398.

Haylock, M., McBride, J., 2001. Spatial Coherence and predictability of Indonesian wet season rainfall. Journal of Climate 14, 3882-3887.

Heim, R.R.Jr., 2002. A review of twentieth-century drought indices used in the United States. Bulletin of the American Meteorological Society 83, 1149–1165.

Hendon, H.H., 2003. Indonesian rainfall variability: impacts of ENSO and local air–sea interaction. Journal of Climate 16, 1775–1790.

Herweijer, C., Seager, R., Cook, E.R., Emile-Geay, J., 2007. North American droughts of the last millennium from a gridded network of tree-ring data. Journal of Climate 20, 1353–1376.

Hoerling, M., Kumar, A., 2003. The perfect ocean for drought. Science 299, 691-694.

Huang, G., Hu, K., Xie, S.-P., 2010. Strengthening of tropical Indian Ocean teleconnection to the Northwest Pacific since the mid-1970s: An atmospheric GCM study. Journal of Climate 23, 5294–5304.

Jiang, D.B., Wang, H.J., 2005. Natural interdecadal weakening of East Asian summer monsoon in the late 20th century. Chinese Science Bulletin 50, 1923–1929

Johnson, N.C., Feldstein, S.B., 2010. The continuum of North Pacific sea level pressure patterns: Intraseasonal, interannual, and interdecadal variability. Journal of Climate 23, 851–867.

Kaplan, A., Cane, M., Kushnir, Y., Clement, A., Blumenthal, M., Rajagopalan, B., 1998. Analyses of global sea surface temperature 1856-1991. Journal of Geophysical Research 103, 18567–18589.

Kim, H.-M., Webster, P.J., Curry, J.A., 2009. Impact of shifting patterns of Pacific Ocean warming on North Atlantic tropical cyclones. Science 325, 77–80.

Krishna Kumar, K., Rajagopalan, B., Cane, M., 1999. On the weakening relationship between the Indian monsoon and ENSO. Science 284, 2156–2159.

Lau, K.-M., Weng, H.Y., 2002. Recurrent Teleconnection Patterns Linking Summertime Precipitation Variability over East Asia and North America. Journal of the Meteorological Society of Japan 806, 1309–1324.

Li, H., Dai, A., Zhou, T., Lu, J., 2010. Responses of East Asian summer monsoon to historical SST and atmospheric forcing during 1950–2000. Climate Dynamics 34, 501–514.

Li, J., Cook, E.R., D'Arrigo, R., Chen, F., Gou, X., 2009a. Moisture variability across China and Mongolia: 1951–2005. Climate Dynamics 32, 1173–1186.

Li, J., et al., 2009b. Summer monsoon moisture variability over China and Mongolia during the past four centuries. Geophysical Research Letters 36, L22705, doi:10.1029/2009GL041162.

Li, J., Cook, E.R., Chen, F., Gou, X., D'Arrigo, R., Yuan, Y., 2010. An extreme drought event in the Tien Shan area in the year 1945. Journal of Arid Environments 74, 1225–1231.

Li, J., Xie, S.-P., Cook, E.R., Huang, G., D'Arrigo, R., Liu, F., Ma, J., Zheng, X.-T., 2011. Interdecadal modulation of El Niño amplitude during the past millennium. Nature Climate Change 1, 114–118.

Li, J., Xie S.-P., Cook, E.R., Morales, M., Christie, D., Johnson, N., Chen, F., D'Arrigo, R., Fowler, A., Gou, X., Fang, K., 2013. El Niño modulations over the past seven centuries. Nature Climate Change 3, 822–826.

Mann, M.E., Rutherford, S., Wahl, E., Ammann, C., 2007. Robustness of proxy-based climate field reconstruction methods. Journal of Geophysical Research 112, D12109, doi:10.1029/2006JD008272.

McGregor, S., Timmermann, A., Timm, O., 2010. A unified proxy for ENSO and PDO variability since 1650. Climate of Past 6, 1–17.

McPhaden, M.J., Zebiak, S.E., Glantz, M.H., 2006. ENSO as an integrating concept in earth science. Science 314, 1740–1745.

Meko, D.M., Stockton, C.W., Boggess, W.R., 1995. The tree-ring record of severe sustained drought. Water Resource Bulletin 31, 789–801.

Mitchell, T.D., Jones, P.D., 2005. An improved method of constructing a database of monthly climate observations and associated high-resolution grids. International Journal of Climatology 25, 693–712.
Notaro, M., Zarrin, A., 2011. Sensitivity of the North American monsoon to antecedent Rocky Mountain snowpack. Geophysical Research Letters 38, L17403, doi:10.1029/2011GL048803.
Ntale, H.K., Gan, T.Y., 2003. Drought indices and their application to East Africa. International Journal of Climatology 23: 1335–1357.
Pal, J.S., Eltahir, E.A.B., 2001. Pathways relating soil moisture conditions to future summer rainfall with a model of the land– atmosphere system. Journal of Climate 14, 1227–1242.
Palmer, W.C., 1965. Meteorological Drought. Weather Bureau Research Paper 45, Washington, D.C.
Rasmusson, E.M., Carpenter, T.H., 1982. Variations in tropical sea surface temperature and surface wind fields associated with the Southern Oscillation/ El Niño. Monthly Weather Review 110, 354–384.
Rayner, N.A., Brohan, P., Parker, D.E., Folland, C.K., Kennedy, J.J., Vanicek, M., Ansell, T., Tett, S.F.B., 2006. Improved analyses of changes and uncertainties in marine temperature measured in situ since the mid-nineteenth century: the HadSST2 dataset. Journal of Climate 19, 446–469.
Ropelewski, C.E., Halpert, M.S., 1987. Global and regional scale precipitation and temperature patterns associated with the El Niño/Southern Oscillation. Monthly Weather Review 115, 1606–1626.
Seager, R., Kushnir, Y., Herweijer, C., Naik, N., Miller, J., 2005. Modeling of tropical forcing of persistent droughts and pluvials over western North America: 1856–2000. Journal of Climate 18, 4065–4088.
Shukla, J., Paolino, D.A., 1983. The Southern Oscillation and long range forecasting of the summer monsoon over India. Monthly Weather Review 111, 1830-1837.
Sinha, A., Berkelhammer, M., Stott, L., Mudelsee, M., Cheng, H., Biswas, J., 2011. The leading mode of Indian Summer Monsoon precipitation variability during the last millennium. Geophysical Research Letters 38, L15703, doi:10.1029/2011GL047713.
Smerdon, J.E., Kaplan, A., Chang, D., Evans, M.N., 2010. A pseudoproxy evaluation of the CCA and RegEM methods for reconstructing climate fields of the last millennium. Journal of Climate 23, 4856–4880.
Smerdon, J. E., Kaplan, A., Zorita, E., González-Rouco, J.F., Evans, M.N., 2011. Spatial performance of four climate field reconstruction methods targeting the Common Era. Geophysical Research Letters 38, L11705, doi:10.1029/2011GL047372.
Smith, T.M., Reynolds, R.W., Peterson, T.C., Lawrimore, J., 2008. Improvements to NOAA's Historical Merged Land-Ocean Surface Temperature Analysis 1880-2006. Journal of Climate 21, 2283–2296.
Stahle, D.W., et al., 1998. Experimental dendroclimatic reconstruction of the Southern Oscillation. Bulletin of the American Meteorological Society 79, 2137–2152.
Stahle, D.W., Fye, F.K., Cook, E.R., Griffin, R.D., 2007. Tree-ring reconstructed megadroughts over North America since AD 1300. Climatic Change 83, 133–149.
Stahle, D.W., et al., 2011. Major Mesoamerican droughts of the past millennium. Geophysical Research Letters 38, L05703, doi:10.1029/2010GL046472.

Stevenson, S., Fox-Kemper, B., Jochum, M., Neale, R., Deser, C., Meehl, G., 2012. Will there be a significant change to El Nino in the 21st Century? Journal of Climate 25, 2129–2145.

St. George, S., Meko, D., Cook, E.R., 2010. The seasonality of precipitation signals embedded within the North American Drought Atlas. Holocene 20, 983–988.

Thompson, L.G., Yao, T., Mosley-Thompson, E., Davis, M.E., Henderson, K.A., Lin, P.-N., 2000. A high-resolution millennial record of the South Asian Monsoon from Himalayanice cores. Science 289, 1916–1919.

Tokinaga, H., Xie, S.-P., Timmermann, A., McGregor, S., Ogata, T., Kubota, H., Okumura, Y.M., 2012. Regional patterns of tropical Indo-Pacific climate change: Evidence of the Walker Circulation weakening. Journal of Climate 25, 1689–1710.

Trenberth, K.E., 1997. The definition of El Niño. Bulletin of the American Meteorological Society 78, 2771–2777.

Trenberth, K.E., Branstator, G.W., Karoly, D., Kumar, A., Lau, N.-C., Ropelewski, C., 1998. Progress during TOGA in understanding and modeling global teleconnections associated with tropical sea surface temperature. Journal of Geophysical Research 103, 14291–14324.

Trenberth, K.E., Stepaniak, D.P., 2001. Indices of El Niño evolution. Journal of Climate 14, 1697–1701.

von Storch, H., Zorita, E., Jones, J.M., Dimitriev, Y., González-Rouco, F., Tett, S.F.B., 2004. Reconstructing past climate from noisy data. Science 306, 679–682.

Wells, N., Goddard, S., Hayes, M.J., 2004. A self-calibrating Palmer drought severity index. Journal of Climate 17, 2335–2351.

Wilson, R., Cook, E.R., D'Arrigo, R., Riedwyl, N., Evans, M., Tudhope, A., Allan, R., 2010. Reconstructing ENSO: the influence of method, proxy data, climate forcing and teleconnections. Journal of Quaternary Science 25, 62–78.

Wittenberg, A.T., 2009. Are historical records sufficient to constrain ENSO simulations? Geophysical Research Letters 36, L12702, doi:10.1029/2009GL038710.

Woodhouse, C.A., Kunkel, K.E., Easterling, D.R., Cook, E.R., 2005. The twentieth-century pluvial in the western United States. Geophysical Research Letters 32, L07701, doi:10.1029/2005GL022413.

Wu, R., Kinter III, J. L., 2009. An analysis of the relationship of U.S. droughts with SST and soil moisture: Distinguishing the time scale of droughts. Journal of Climate 22, 4520–4538.

Xie, S.-P., Hu, K., Hafner, J., Tokinaga, H., Du, Y., Huang, G., Sampe, T., 2009. Indian Ocean capacitor effect on Indo-western Pacific climate during the summer following El Nino. Journal of Climate 22, 730–747.

Xie, S.-P., Du, Y., Huang, G., Zheng, X.-T., Tokinaga, H., Hu, K., Liu, Q., 2010. Decadal shift in El Nino influences on Indo-western Pacific and East Asian climate in the 1970s. Journal of Climate 23, 3352–3368.

Yeh, S.-W., Kirtman, B.P., Kug, J.-S., Park, W., Latif, M., 2011. Natural variability of the central Pacific El Niño event on multi-centennial timescales. Geophysical Research Letters 38, L02704, doi:10.1029/2010GL045886.

Yu, J.-Y., Kim, S.T., 2010. Identification of Central-Pacific and Eastern-Pacific types of ENSO in CMIP3 models. Geophysical Research Letters 37, L15705, doi:10.1029/2010GL044082.

Zhang, P., et al., 2008. A test of climate, sun, and culture relationships from an 1810-year Chinese cave record. Science 322, 940–942.

Zhao P., Yang, S., Wang, H., Zhang, Q., 2011. Interdecadal Relationships between the Asian–Pacific Oscillation and Summer Climate Anomalies over Asia, North Pacific, and North America during a Recent 100 Years. Journal of Climate 24, 4793–4799.

Zhou, T., Yu, R., Li, H., Wang, B., 2008. Ocean forcing to changes in global monsoon precipitation over the recent half century. Journal of Climate 21, 3833–3852.

**Figure Captions:**

Fig. 1. Composite mean and standard deviation of monthly Niño3.4 indices, based on SST anomalies for 20 observed El Niño events during 1950-2011. El Niño events are defined according to the criteria that maximum warming in the Niño3.4 region during the months of November-January (NDJ) exceeds 0.5°C. Anomalies are relative to the 1971-2000 base period.

Fig. 2. Map of Asia and North America showing the locations of the reconstructed PDSI grid points in MADA and NADA.

Fig. 3. Number (A) and percentage (B) of reconstructed grip points available back in time in MADA and NADA.

Fig. 4. Spatial pattern of the first two EOFs of MADA and NADA.

Fig. 5. Principal components of the first and second EOF mode for MADA and NADA during 1300-2005. Bold line denotes a 15-year low-pass filter for each series.

Fig. 6. Spatial correlations with global SSTs for MADA PC1 (A-F) and MADA PC2 (G-L) during 1870-2005. Left (right) box in each panel denotes the Niño4 (Niño3) region, respectively. The correlation coefficient at the 0.05 significance level is about 0.17, based on a two-tailed student's t-test.

Fig. 7. Same as in Fig. 6, but for NADA PC1 (A-F) and NADA PC2 (G-L).

Fig. 8. Lead-lag correlations with Niño3 (blue) and Niño4 (red) index for MADA PC1 (A), MADA PC2 (B), and NADA PC1 (C). The common period for calculating the correlations is 1870-2005. The dashed lines denote the 0.05 significance level, based on a two-tailed student's t-test.

Fig. 9. Spatial correlations of MADA PC1 with seasonal precipitation (A-F) and temperature (G-L) during 1951-2005. Contours overlapped in A-F denote the ratio of seasonal to annual rainfall over the region. The correlation coefficient at the 0.05 significance level is about 0.27, based on a two-tailed student's t-test.

Fig. 10. Same as in Fig. 9, but for MADA PC2.

Fig. 11. Same as in Fig. 9, but for NADA PC1.

Fig. 12. Running 31-year Spearman's rank correlations of NADA PC1 with MADA PC1/PC2 over 1301-2005. Note that the y-axis for MADA PC2 was flipped in order to make its correlations visually comparable to those of MADA PC1. The dashed line denotes the 0.05 significance level, based on a two-tailed student's t-test.

**Table 1.** Cross correlations of the MADA and NADA PCs over the common period 1301-2005. Bold values are significant at the 0.05 levels, based on a two-tailed student's t-test.

| | MADA PC1 | MADA PC2 | NADA PC1 | NADA PC2 |
|---|---|---|---|---|
| MADA PC1 | 1.00 | | | |
| MADA PC2 | **-0.33** | 1.00 | | |
| NADA PC1 | **0.18** | **-0.22** | 1.00 | |
| NADA PC2 | **-0.10** | 0.06 | 0.00 | 1.00 |

**Figure 1**

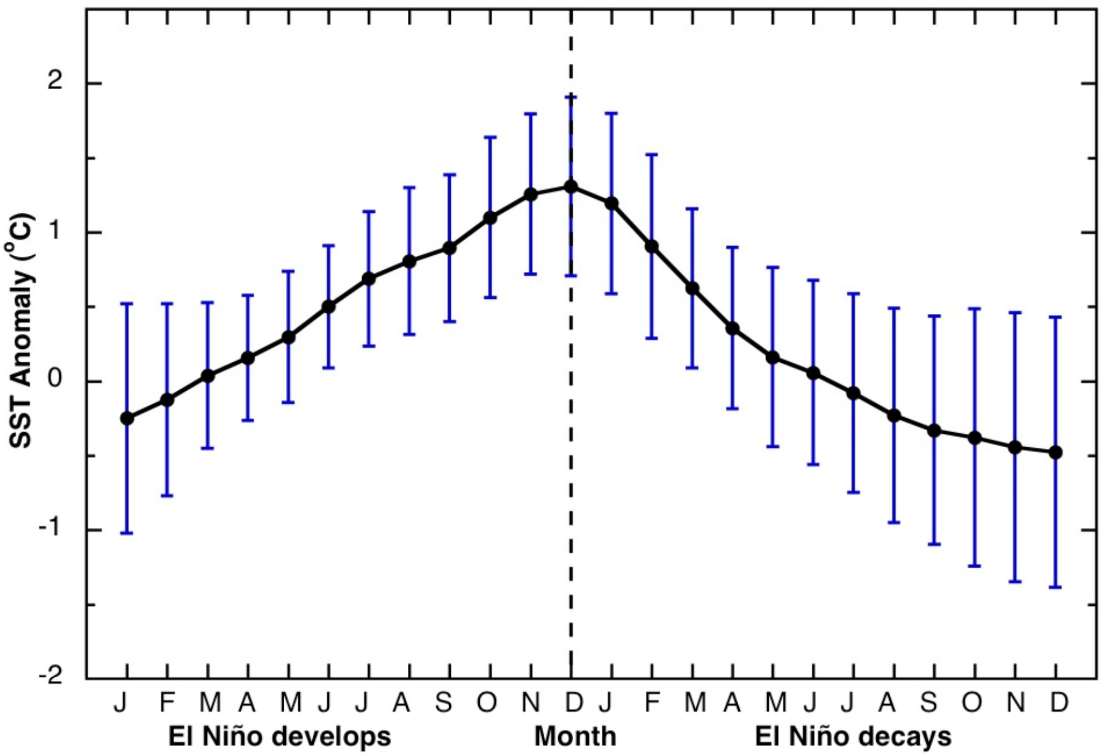

SST Anomaly (°C)
2
1
0
-1
-2
J F M A M J J A S O N D J F M A M J J A S O N D
El Niño develops
Month
El Niño decays

**Figure 2**

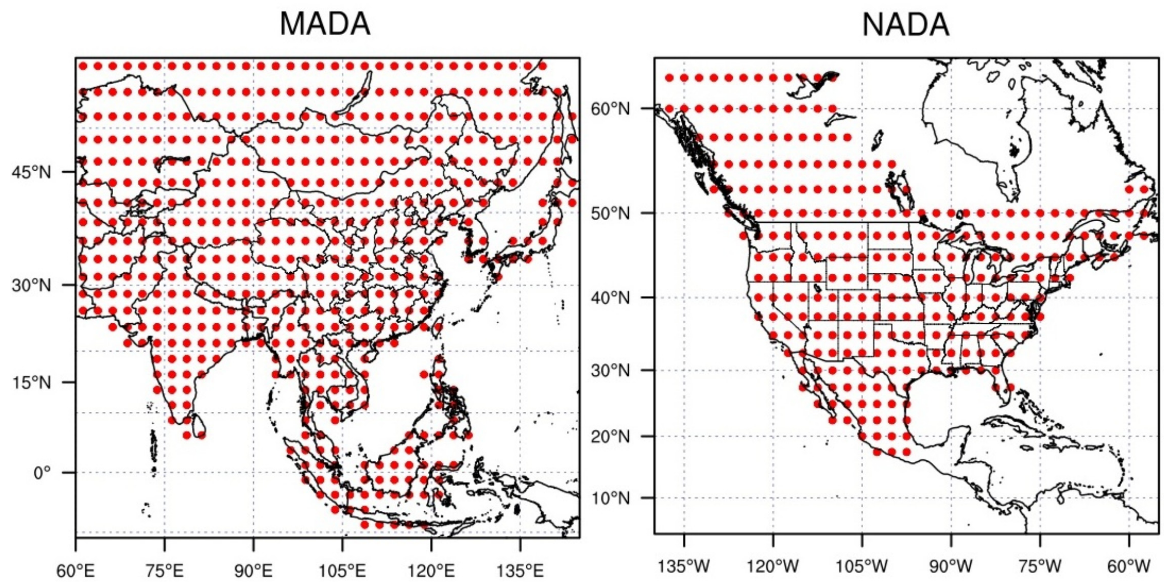
MADA
NADA
45°N
30°N
15°N
0°
60°E
75°E
90°E
105°E
120°E
135°E
60°N
50°N
40°N
30°N
20°N
10°N
135°W
120°W
105°W
90°W
75°W
60°W

**Figure 3**

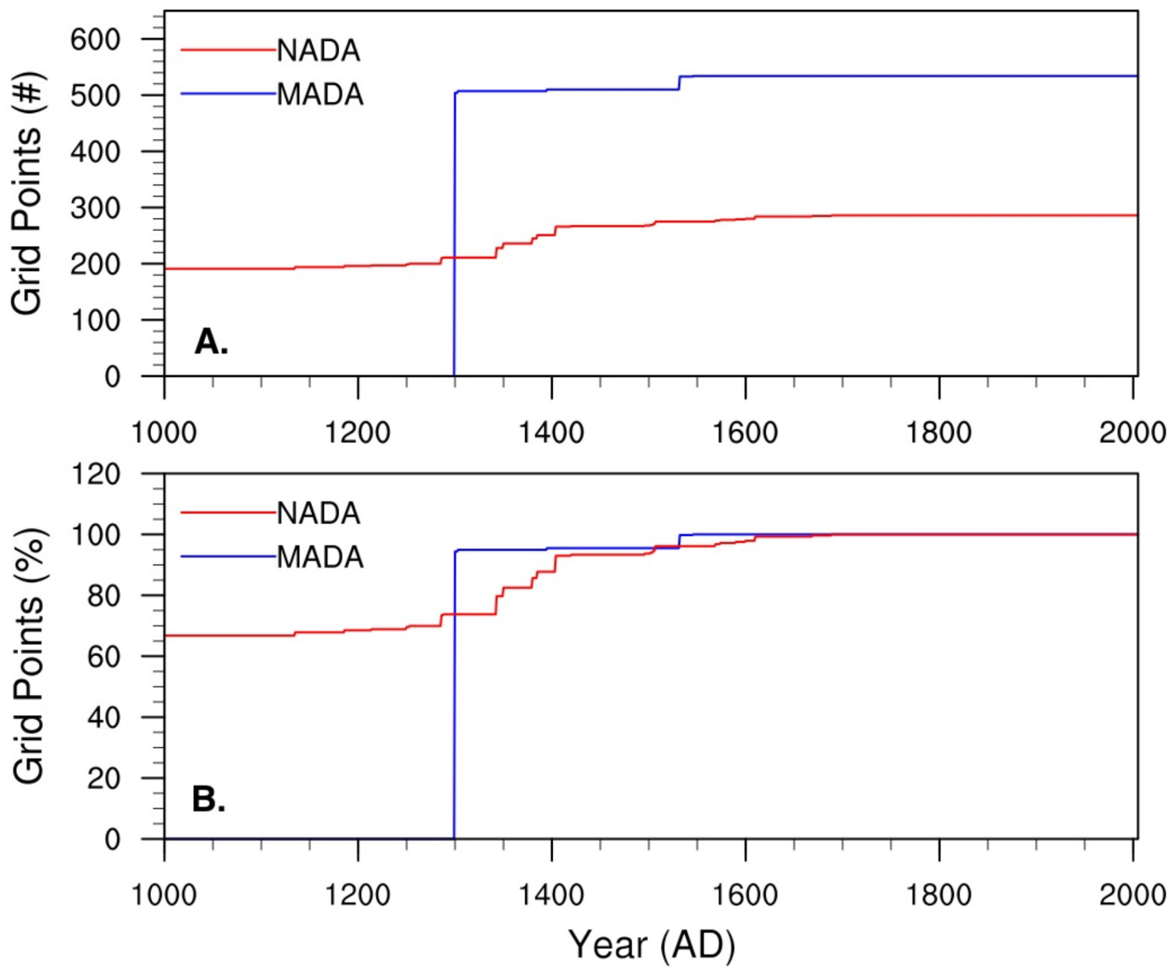

NADA
MADA
Grid Points (#)
600
500
400
300
200
100
0
A.
1000
1200
1400
1600
1800
2000
NADA
MADA
Grid Points (%)
120
100
80
60
40
20
0
B.
1000
1200
1400
1600
1800
2000
Year (AD)

**Figure 4**

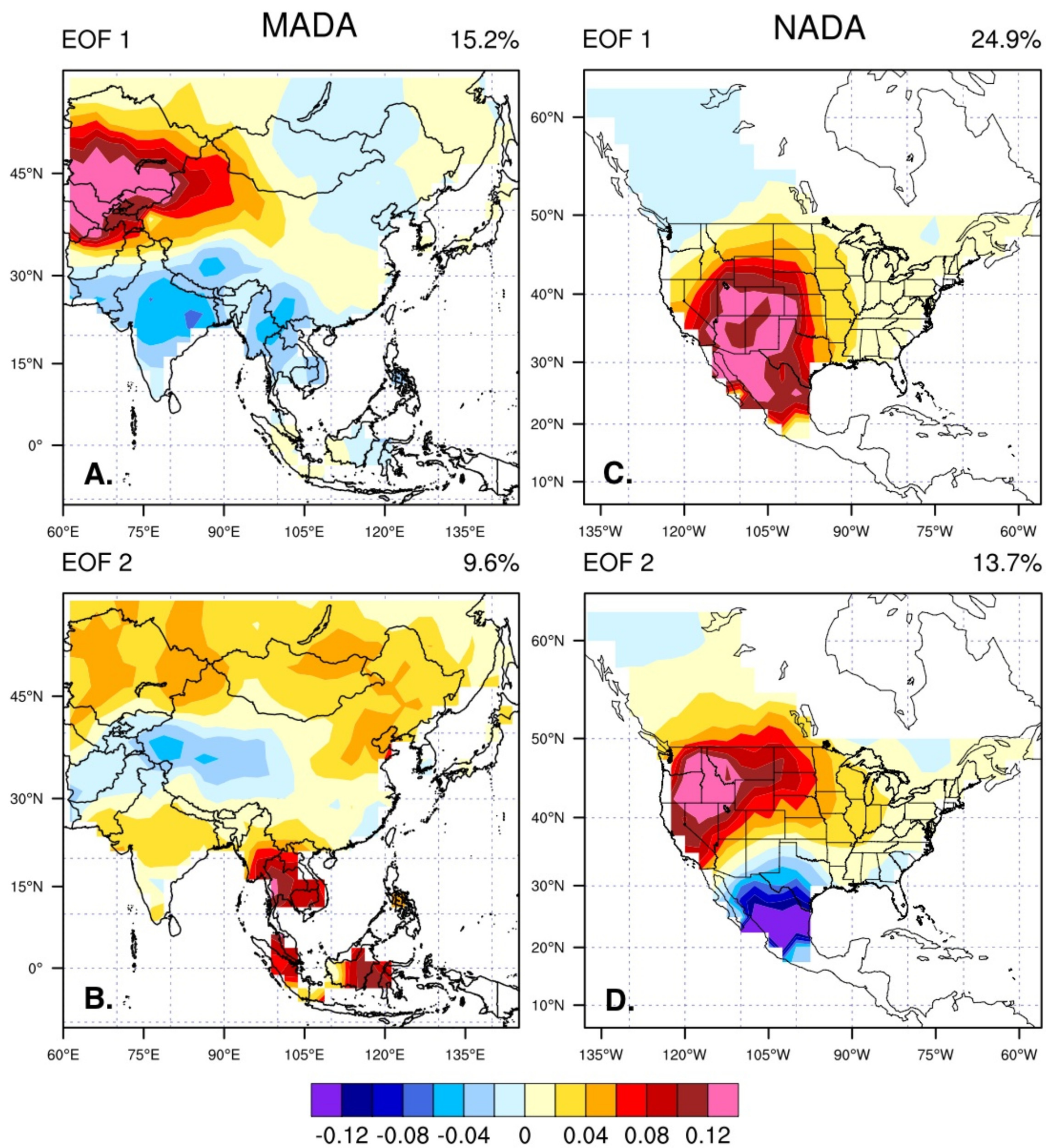

MADA
NADA
EOF 1
15.2%
EOF 1
24.9%
A.
C.
EOF 2
9.6%
EOF 2
13.7%
B.
D.
60°E
75°E
90°E
105°E
120°E
135°E
45°N
30°N
15°N
0°
135°W
120°W
105°W
90°W
75°W
60°W
60°N
50°N
40°N
30°N
20°N
10°N
-0.12 -0.08 -0.04 0 0.04 0.08 0.12

**Figure 5**

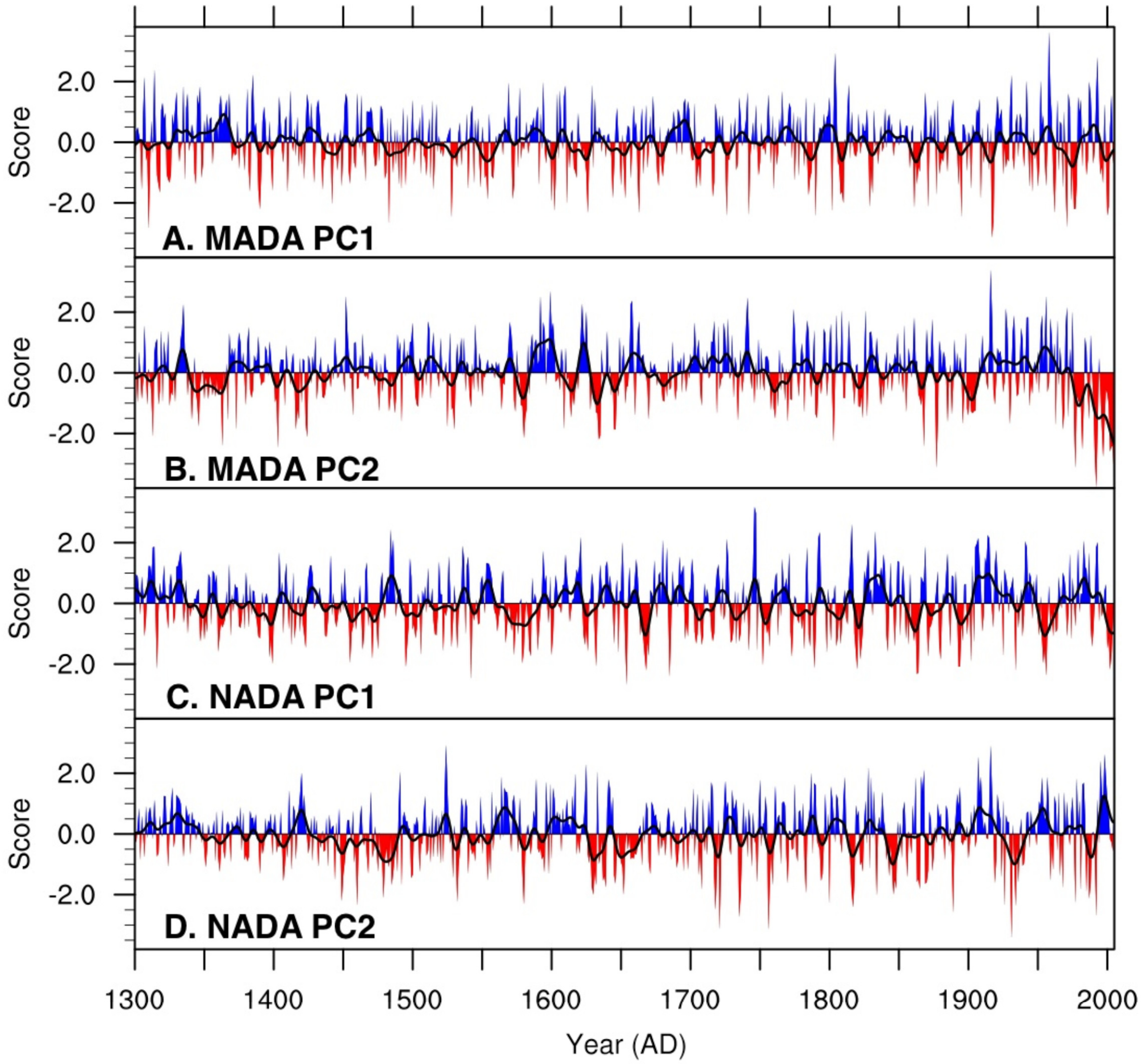

A. MADA PC1
B. MADA PC2
C. NADA PC1
D. NADA PC2
Score
2.0
0.0
-2.0
1300
1400
1500
1600
1700
1800
1900
2000
Year (AD)

**Figure 6**

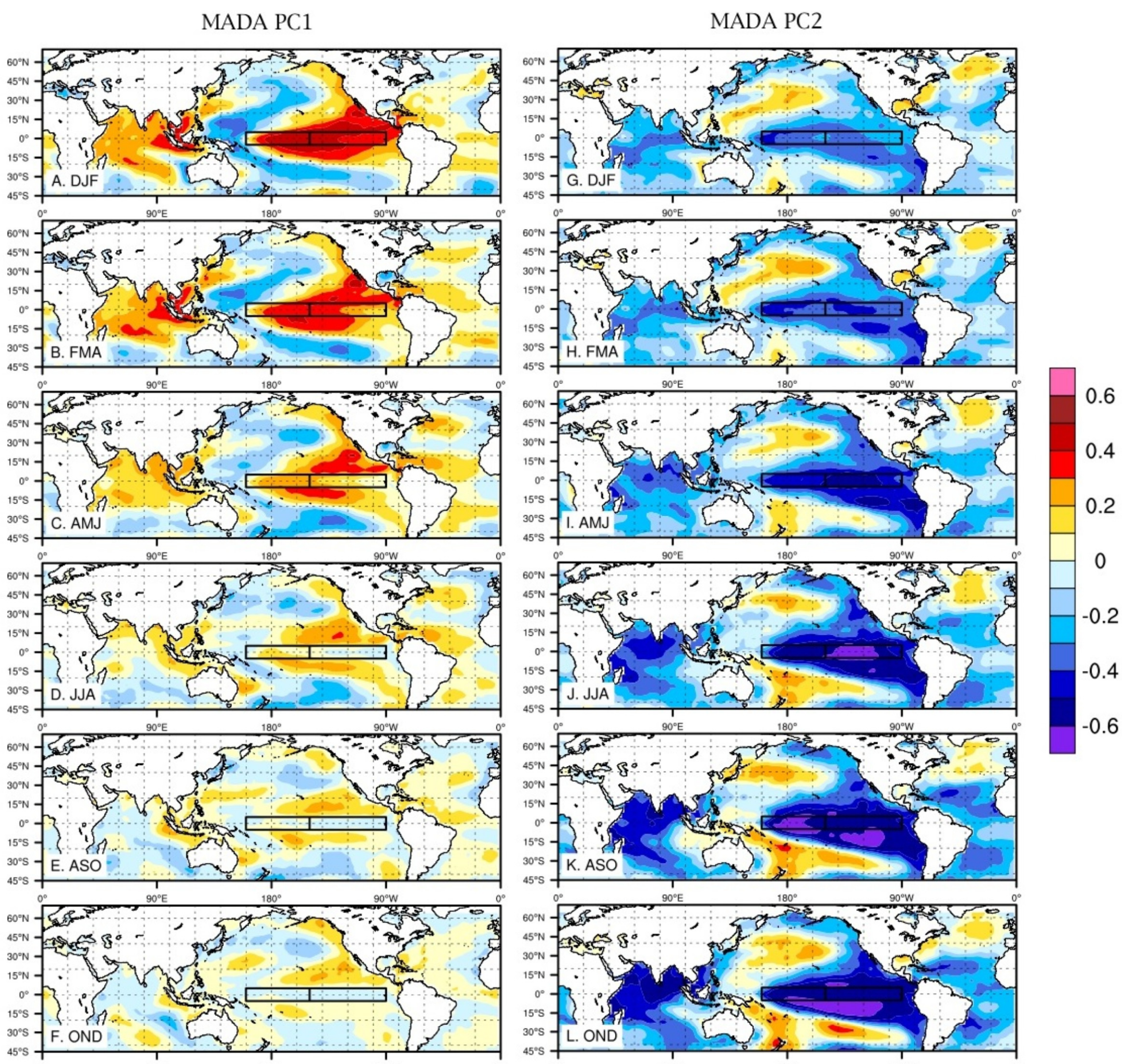

MADA PC1
MADA PC2
A. DJF
B. FMA
C. AMJ
D. JJA
E. ASO
F. OND
G. DJF
H. FMA
I. AMJ
J. JJA
K. ASO
L. OND
60°N
45°N
30°N
15°N
0°
15°S
30°S
45°S
0°
90°E
180°
90°W
0.6
0.4
0.2
0
-0.2
-0.4
-0.6

**Figure 7**

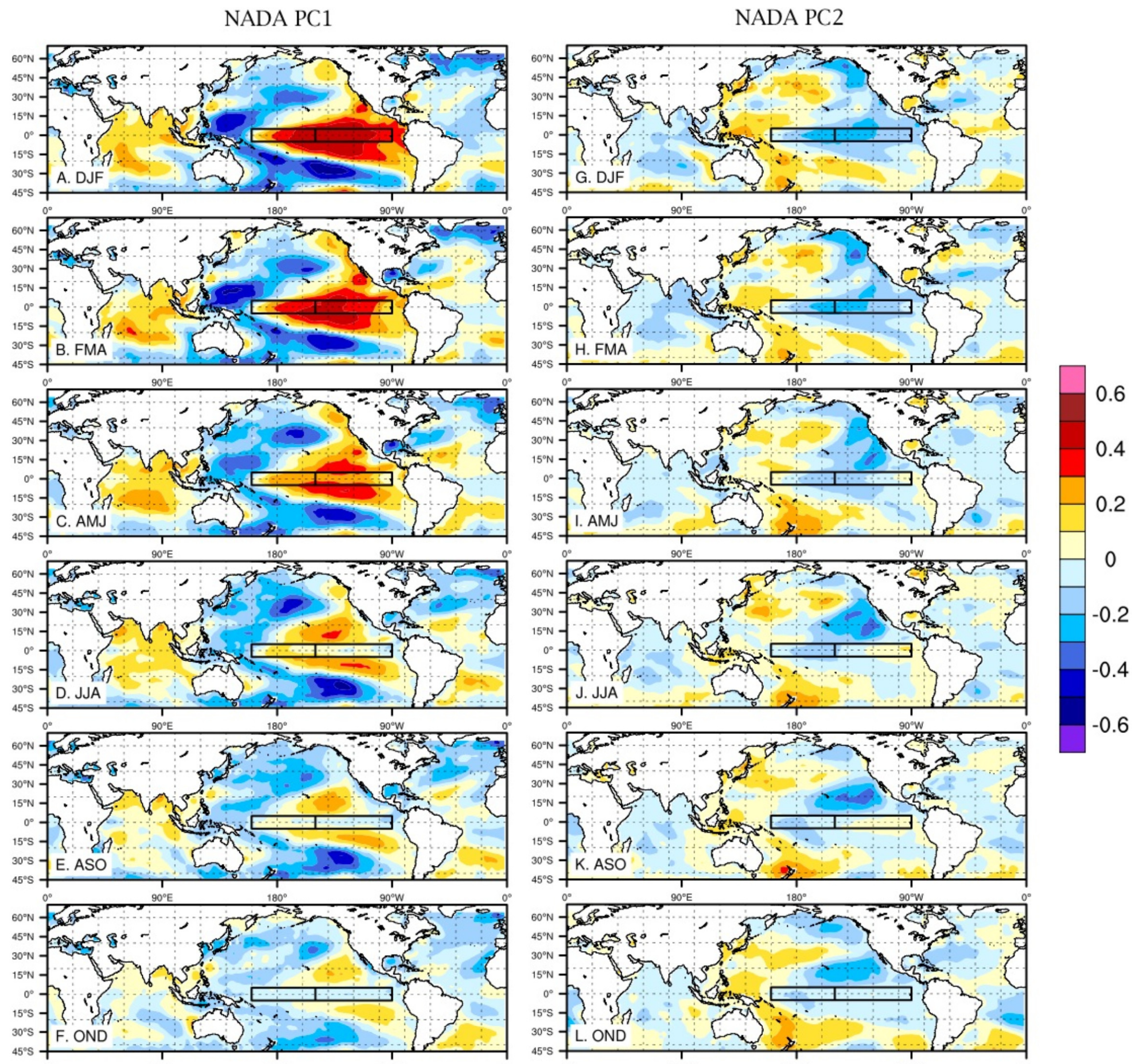

NADA PC1
NADA PC2
A. DJF
B. FMA
C. AMJ
D. JJA
E. ASO
F. OND
G. DJF
H. FMA
I. AMJ
J. JJA
K. ASO
L. OND
0.6
0.4
0.2
0
-0.2
-0.4
-0.6

**Figure 8**

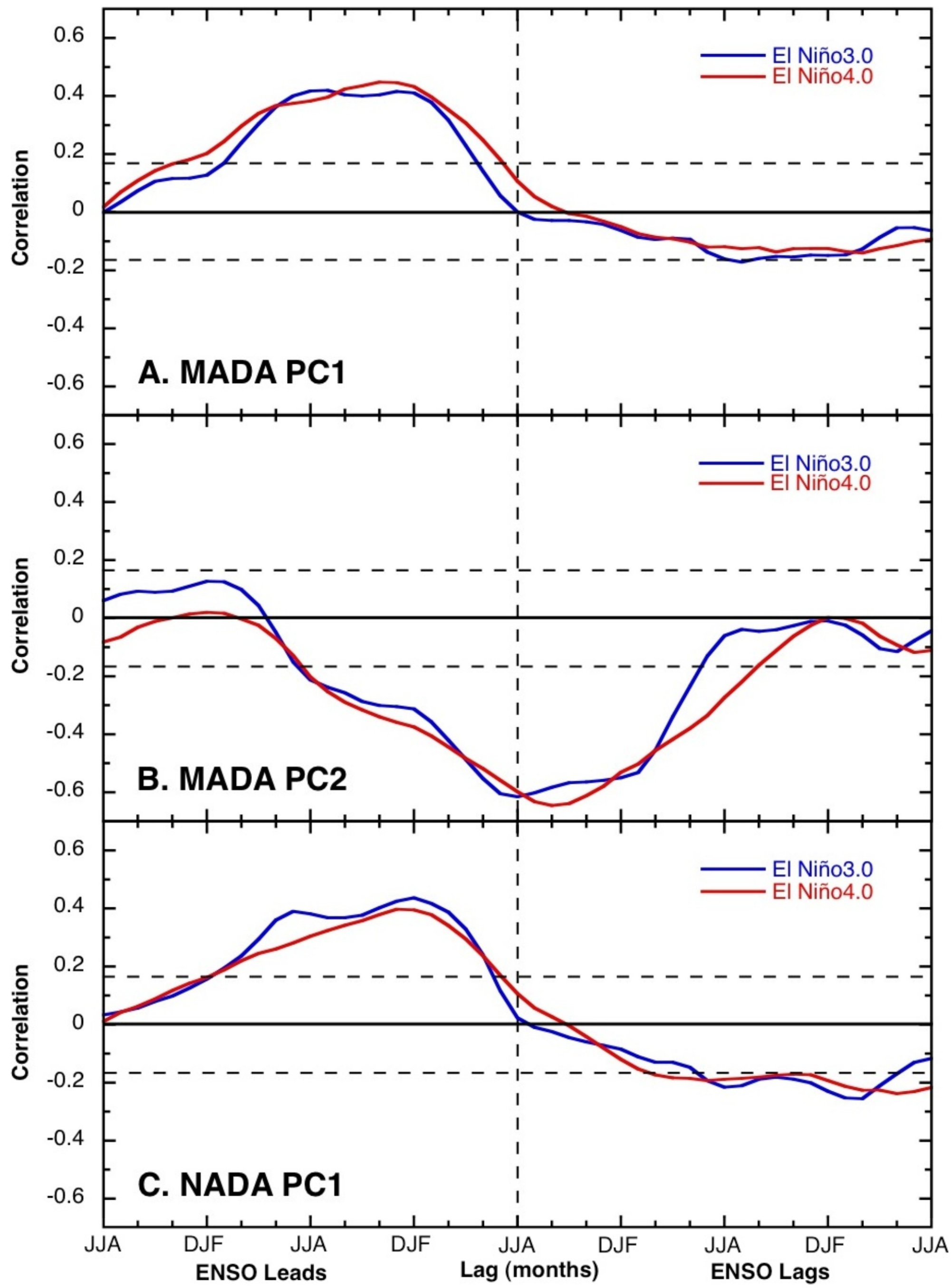

El Niño3.0
El Niño4.0
A. MADA PC1
B. MADA PC2
C. NADA PC1
Correlation
0.6
0.4
0.2
0
-0.2
-0.4
-0.6
JJA
DJF
JJA
DJF
JJA
DJF
JJA
DJF
JJA
ENSO Leads
Lag (months)
ENSO Lags

**Figure 9**

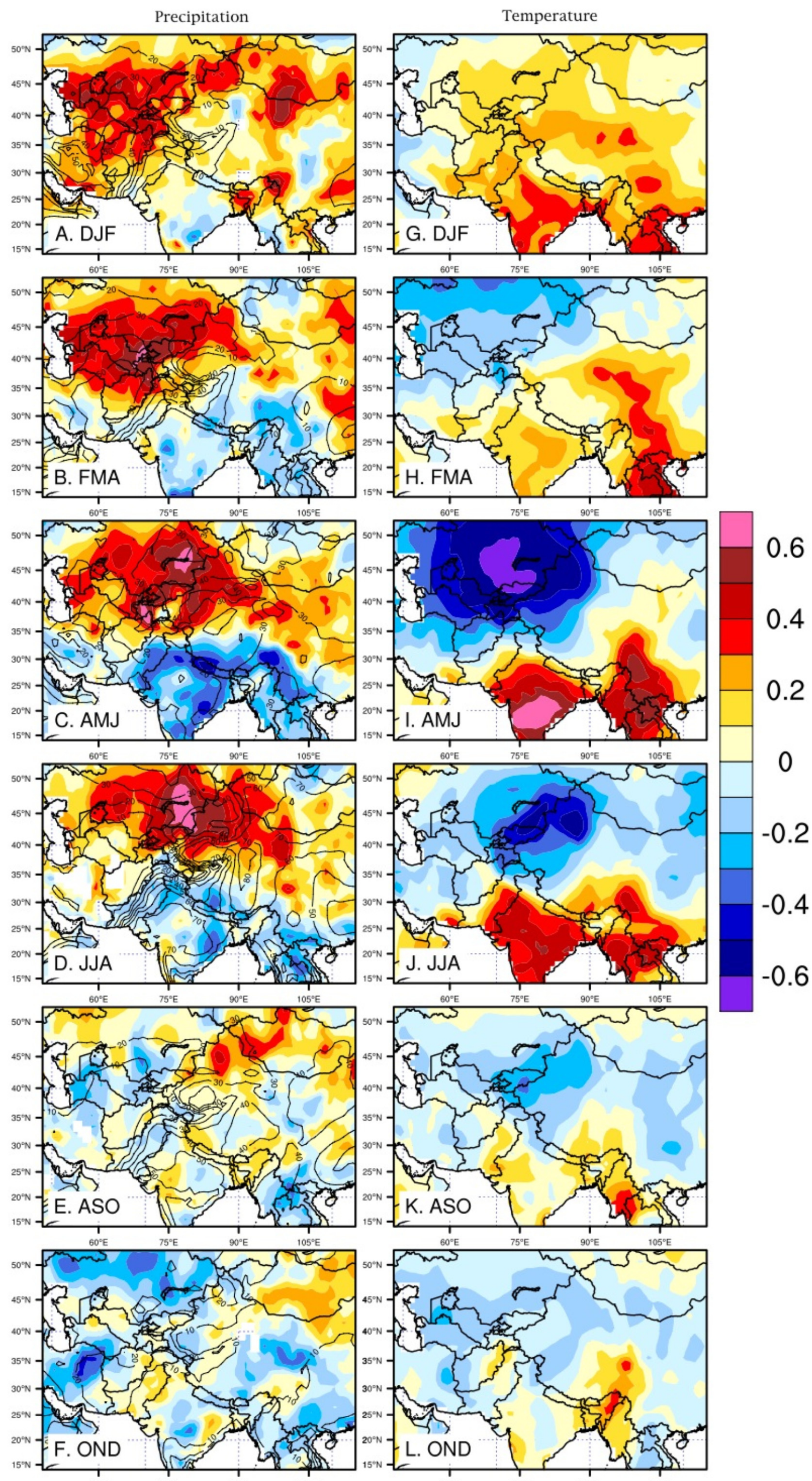

Precipitation
Temperature
A. DJF
B. FMA
C. AMJ
D. JJA
E. ASO
F. OND
G. DJF
H. FMA
I. AMJ
J. JJA
K. ASO
L. OND
0.6
0.4
0.2
0
-0.2
-0.4
-0.6

1 **Figure 10**

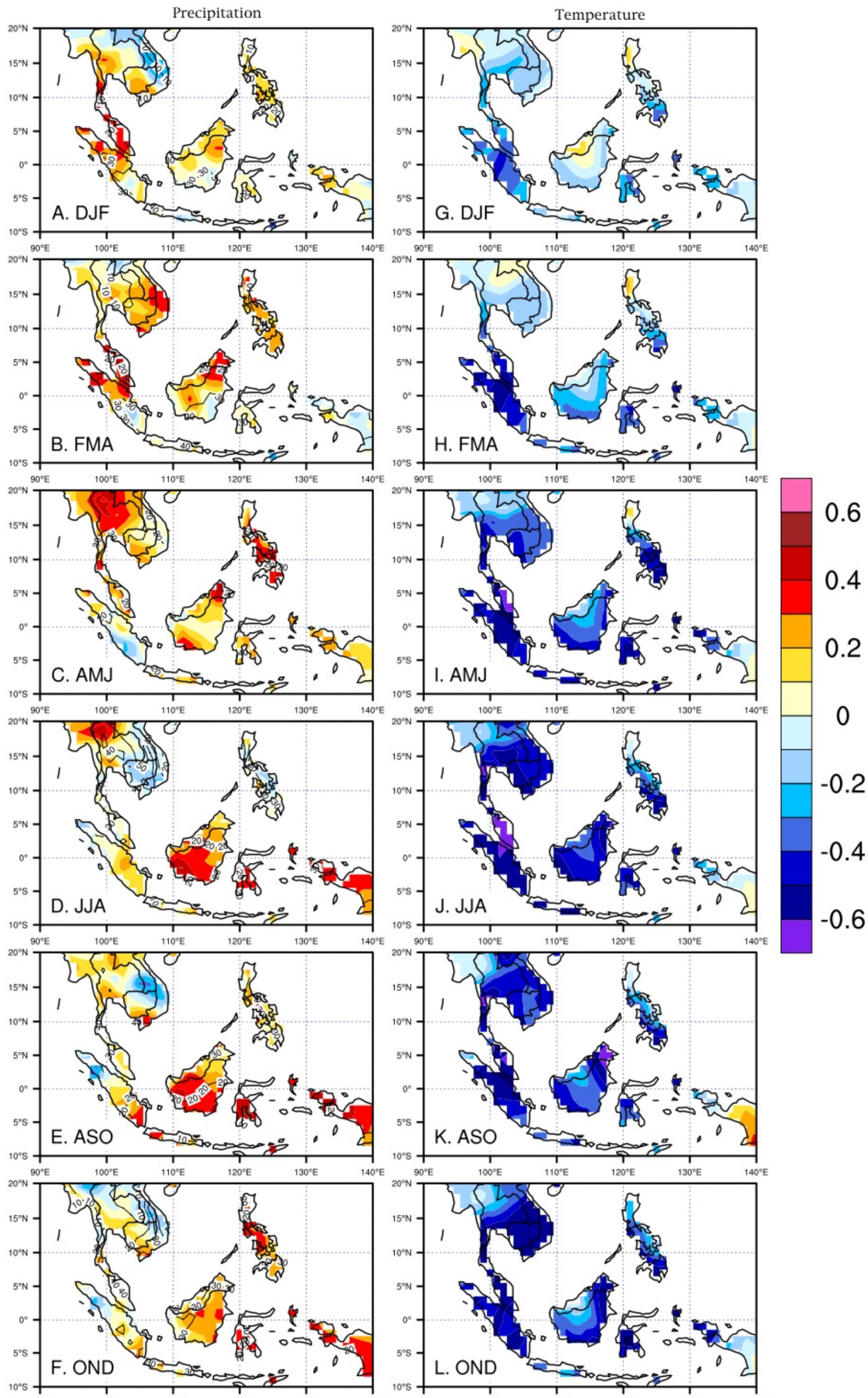

Precipitation
Temperature
A. DJF
B. FMA
C. AMJ
D. JJA
E. ASO
F. OND
G. DJF
H. FMA
I. AMJ
J. JJA
K. ASO
L. OND
0.6
0.4
0.2
0
-0.2
-0.4
-0.6


2

**Figure 11**

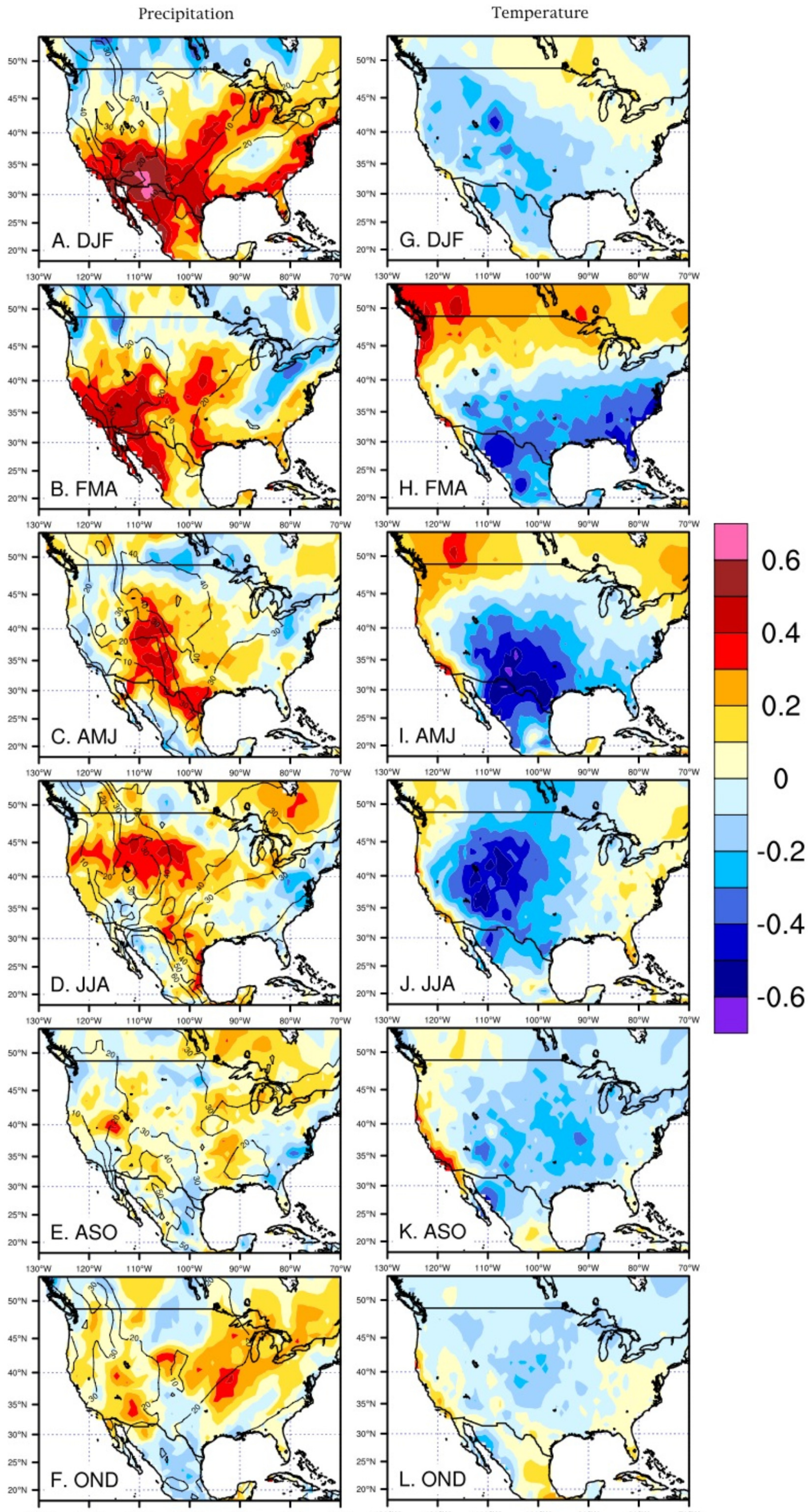
Precipitation
Temperature
A. DJF
B. FMA
C. AMJ
D. JJA
E. ASO
F. OND
G. DJF
H. FMA
I. AMJ
J. JJA
K. ASO
L. OND
0.6
0.4
0.2
0
-0.2
-0.4
-0.6

**Figure 12**

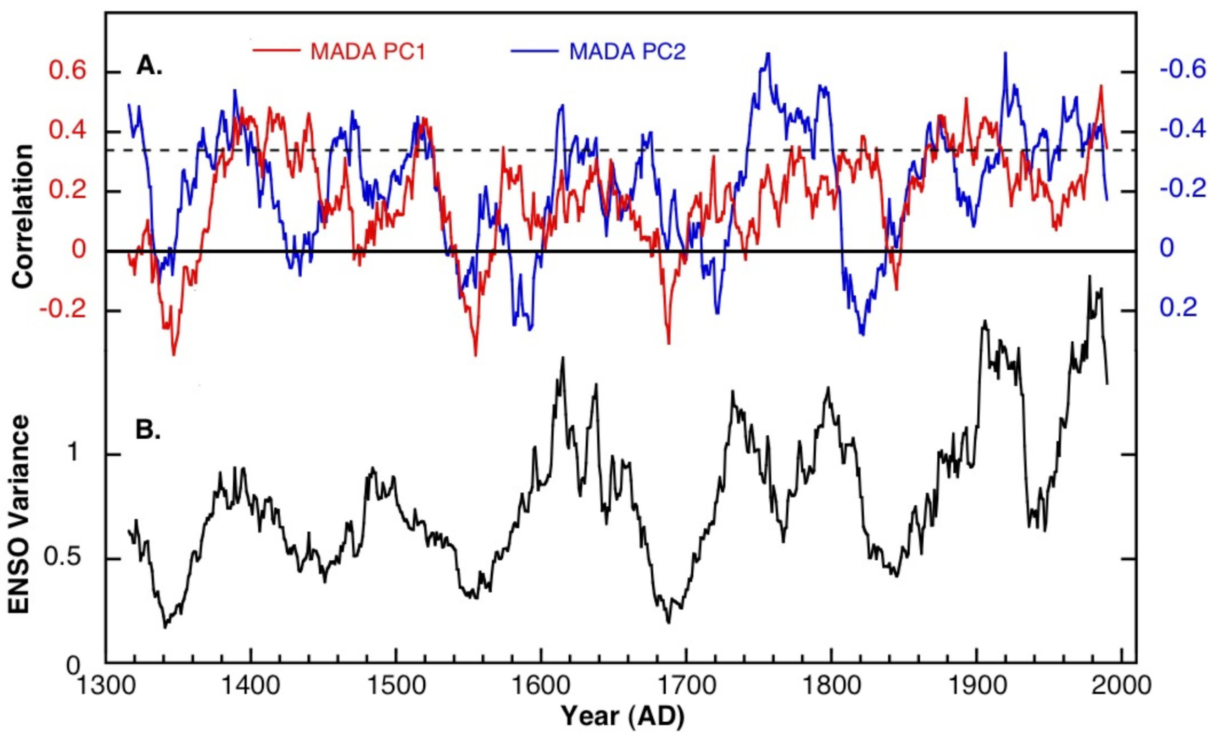

A.
MADA PC1
MADA PC2
Correlation
0.6
0.4
0.2
0
-0.2
-0.6
-0.4
-0.2
0
0.2
B.
ENSO Variance
1
0.5
0
1300
1400
1500
1600
1700
1800
1900
2000
Year (AD)